

Neural Network-Assisted Fiber Tracking of Synthetic and White Matter DT-MR Images

L.M. San-José-Revuelta, M. Martín-Fernández and C. Alberola-López *

Abstract—In this paper, a recently developed fiber tracking algorithm to be used with diffusion tensor (DT) fields acquired via magnetic resonance imaging (MRI) is improved and applied to real brain DT-MR images. The method performs satisfactorily in regions where branching and crossing fibers exist and offers the capability of reporting a probability value for the computed tracts. This certainty figure takes into account both the anisotropy and the information provided by *all* the eigenvectors and eigenvalues of the diffusion matrix at each voxel. In previous papers of the authors, a simpler algorithm was applied only to elementary synthetic DT-MR images. As now presented, this algorithm is now adequately used with more intricate synthetic images and is applied to real white matter DT-MR images with successful results. A novel neural network is used to estimate the main parameters of the algorithm. Numerical experiments show a performance gain over previous approaches, specially with respect to convergence and computational load. The tracking of white matter fibers in the human brain will improve the diagnosis and treatment of many neuronal diseases.

Keywords: *diffusion tensor magnetic resonance imaging, fiber tracking, neural network*

1 Introduction

The technique of Diffusion Tensor Magnetic Resonance Imaging (DT-MRI) measures the diffusion of hydrogen atoms within water molecules in 3D space. Since in cerebral white matter most random motion of water molecules are restricted by axonal membranes and myelin sheets, diffusion anisotropy allows depiction of directional anisotropy within neural fiber structures [4, 1]. The DT-MRI technique has raised great interest in the neuroscience community for a better understanding of the fiber tract anatomy of the human brain. Though this field of search is still in its early stages, its development is growing very fast.

There exist many important applications for white matter tractography: brain surgery (knowing the extension of the fiber bundles could minimize the functional damage to the patient), white matter visualization using fiber

traces (for a better understanding of brain anatomy) and inference of connectivity between different parts of the brain (useful for functional and morphological research of the brain).

Apart from a very few approaches for direct volume rendering [8], the great majority of DT-MRI visualization techniques focuses on the integration of sample points along fiber trajectories and their three-dimensional representation [9]. These approaches usually only use the principal eigenvector of the diffusion ellipsoid as an estimate of the predominant direction of water diffusion [4].

However, due to both some deficiencies in these tracking methods and several shortcomings inherent in datasets (such as noise, artifacts or partial voluming), these algorithms may depict fiber tracts which do not exist in reality or miss to visualize important connectivity features, e.g. branching structures. In order to avoid misinterpretations, the viewer must be provided with some information on the uncertainty of every depicted fiber and of its presence in a certain location. In [10, 11] we proposed an estimation algorithm that takes into account the whole information provided by the diffusion matrix, i.e., it does not only consider the principal eigenvector direction but the complete 3D information about the certainty of continuing the path through every possible future direction.

Since in [10, 11] we presented an initial version of our work, numerical simulations were only performed on simple DT-MR synthetic images. The algorithm also includes a procedure that adapts on-line the number of *offspring paths* emerging from the actual voxel, to the degree of anisotropy observed in its proximity. This strategy has been proved to enhance the estimation robustness in areas where multiple fibers cross while it keeps complexity to a moderate level. Besides, a neural Network (NN) is now proposed to adjust the parameters of the algorithm in a user-directed training stage. The detailed study of convergence depending on the strategy used to create the pool of “future seeds” is new in this paper, as well.

For the sake of brevity, the reader interested in the review of previous related approaches can see the corresponding sections in [2, 3, 10].

*ETSI Telecomunicación, University of Valladolid, 47010 Valladolid, Spain. Tel: +34-983-423660, Fax: +34-983-423667. Email: lsanjose@tel.uva.es.

2 Tracking Algorithm Description

The basic version of the algorithm used in this paper was first described in [10]. Thus, this section just presents a summary of the method, with special emphasis on the new aspects. The algorithm uses probabilistic criteria and iterates over several points in the analyzed volume (the points given by the highest probabilities in the previous iteration). The process starts in a user-selected seed voxel, V_0 .

At every iteration, the method evaluates a set of parameters related to the central voxel of a cubic structure similar to that shown in Figure 1, left. The central point, V_c , (No. 14 in the figure) represents the last point of the tract being analyzed. In the first iteration, $V_c = V_0$.

2.1 Basic concepts

First, a measure P_i , $i \in \{\text{valid points}\}$, is evaluated based on the probability of going from voxel V_c to voxel V_i . This probability takes into account the eigenvalues and eigenvectors available at point V_c from the DT-MR image diffusion matrix. In order to calculate this probability, the information shown in Fig. 1, right, is used.

The table shows, for every voxel shown in Fig. 1, left, the changes that must occur in indices (m, n, p) , when a tract goes from voxel V_c to voxel V_i . For instance: when going from point No. 14 to point No. 6, coordinate m reduces by 1, n remains the same, and p increases by 1. This is represented in the table with " $\pi_m \pi_n \pi_p = (-0+)$ ". With this information, the probability of each possible destination V_i can be calculated taking into account the projection of each of the eigenvectors to each of the directions defined in the triplet $\pi_m \pi_n \pi_p$. Besides, each projection is weighted by the corresponding eigenvalue λ . Thus, in the previous example, P_i should be calculated as $P_i = V_{1y}\lambda_1 + V_{2y}\lambda_2 + V_{3y}\lambda_3 + V_{1z}\lambda_1 + V_{2z}\lambda_2 + V_{3z}\lambda_3$, where $V_{j\alpha}$ represents the α -component of eigenvector j , $1 \leq j \leq 3$, $\alpha \in \{x, y, z\}$.

The axes reference criterion for the (x, y, z) vector components is also shown in Fig. 1. Note that, for this calculus, the sign "-" in the triplet is equivalent to sign "+". In order to properly calculate P_i , it must be weighed by 0.33 if there are no zeros in triplet i , and by 0.5 if there is one zero.

2.2 Anisotropy and local probability

The following anisotropy index is used in the algorithm:

$$fa = \sqrt{\frac{(\lambda_1 - \lambda_2)^2 + (\lambda_2 - \lambda_3)^2 + (\lambda_1 - \lambda_3)^2}{2(\lambda_1^2 + \lambda_2^2 + \lambda_3^2)}}, \quad (1)$$

where $\lambda_1 \geq \lambda_2 \geq \lambda_3$. When both $fa(V_c)$ and $fa(V_i)$ do not exceed a certain threshold, then point V_i is eliminated as a possible destination point.

Taking into account both P_i and the anisotropy given by Eq. (1), the local probability of voxel i is defined as

$$P'_i = a \cdot \mu_1 \cdot fa(V_i) + (1 - a) \cdot \mu_2 \cdot P_i, \quad 0 < a < 1 \quad (2)$$

where parameter a allows the user to give a higher relative weight to either the anisotropy or the local probability, and μ_1 and μ_2 are scaling factors (normally, 1 and 1000, respectively). The set of values P'_i is properly normalized so that they can be interpreted as probabilities.

2.3 Eigenvectors and direction considerations

Besides these considerations, the final probability of voxel i makes also use of the so-called *smoothness parameters* (described in [7]) which judge the coherence of fiber directions among the trajectories passing through voxel V_c . The mathematical expressions of these four parameters, $\{sp_i\}_{i=1}^4$, as well as their geometrical meaning, is explained in [10]. They measure the angles between the directions that join successive path points, as well as the angles between these directions and the eigenvectors associated to the largest eigenvalues found in those voxels. sp_2, sp_3 and sp_4 are used to maintain the local directional coherence of the estimated tract and avoid the trajectory to follow unlikely pathways [7]. The threshold for sp_1 is set such that the tracking direction could be moved forward consistently and smoothly, preventing the computed path from sharp transitions.

Next, the following parameter is calculated for every valid point whose smoothness parameters satisfy the four corresponding threshold conditions,

$$P''_i = b(\xi_1 sp_1 + \xi_2 sp_2 + \xi_3 sp_3 + \xi_4 sp_4) + (1 - b)P'_i \quad (3)$$

where, ξ_1, ξ_2, ξ_3 and ξ_4 are the corresponding weights of the smoothness parameters (normally, 0.25), and b stands for a weighting factor.

2.4 Path probabilities

Probabilities P''_i can be recursively accumulated, yielding the probability of the path generated by the successive values of V_c ,

$$P_p(k) = P'''_i \cdot P_p(k - 1) \quad (4)$$

with k being the iteration number, and $P'''_i = P''_i / \sum_i P''_i$.

At the end of the visualization stage, every estimated path is plotted with a color that depends on its probability P_p .

2.5 Final criterion and pool of "future seeds"

A pool of voxels is formed by selecting, at the end of each iteration, the s best voxels according to Eq. (3). The

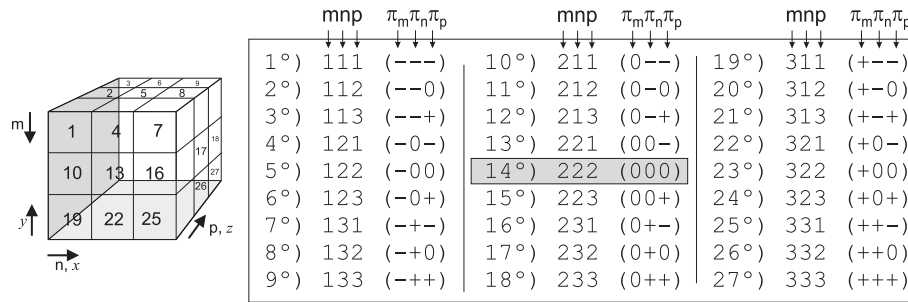


Figure 1: Modifications of indices (m, n, p) when moving from V_c to the neighboring voxel V_i , $1 \leq i \leq 27$, $i \neq 14$.

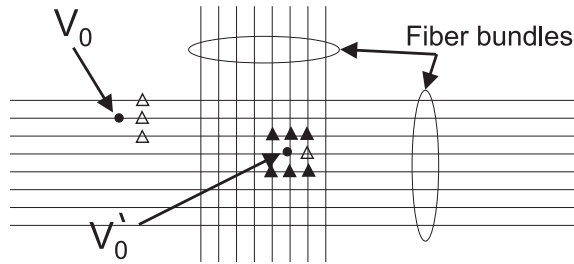


Figure 2: Selection of seeds around V_c for different anisotropies.

first voxel of the pool becomes the central voxel V_c at next iteration, expanding, this way, the current pathway.

As proposed in [11], the value of s is adjusted depending on the degree of anisotropy found in current voxel V_c and its surroundings. When this anisotropy is high, it means that a high directivity exists in that zone, and the probability that V_c belongs to a region where fibers cross is really low. Consequently, s takes a small value (1, 2 or 3). On the other hand, if V_c is found to be situated in a region of high anisotropy, the probabilities of having fibers crossing or branching is higher. In this case, it is interesting to explore various paths starting in V_c . This can be achieved by setting parameter s to a higher value.

This idea is illustrated in Fig. 2, where point V_0 belongs to a very anisotropic region. In this case, the pool of surviving voxels should be augmented with those points marked with a white filled triangle. On the other hand, points like V'_0 , which are situated in a region where two orthogonal fiber bundles cross, have a small anisotropy. In this case, all the points marked with black triangles could be added to the pool in order to be considered as seeds in future iterations.

2.6 Neural network for parameter estimation

Optionally, a neural network with 4 hidden layers and the backpropagation algorithm for learning can be used to adjust the parameters of the algorithm

($a, b, \mu_1, \mu_2, \xi_1, \xi_2, \xi_3, \xi_4$). When this strategy is used, the user is requested to assign a certainty value to the paths automatically generated. This is useful when the algorithm is applied to a different part of the brain (fiber bundles) or even to the same portion but having been scanned with under different conditions. In these cases, the volume of interest will have a different smoothness and anisotropy characterization. To our knowledge, no previous work has proposed any mechanism to estimate the parameters and they are always heuristically adjusted.

3 Numerical Results

In order to evaluate the tracking properties of the proposed algorithm, we have used both synthetic and real DT-MR images.

3.1 Synthetic images

First, four different synthetic DT-MRI data in a $50 \times 50 \times 50$ grid have been generated (see Fig. 3). The first three images (“cross”, “earth” and “log”) were used for testing in [10, 11], while the most complex one –Fig. 3, bottom-right– is new. To make the simulated field more realistic, Rician noise [6] was added in the diffusion weighted images which were calculated from the Stejskal-Tanner equation using the gradient sequence in [12] and a b -value of 1000.

The desired noisy synthetic diffusion tensor data was obtained using an analytic solution to the Stejskal-Tanner equation. Satisfactory tracing results for the first three cases can be found in [10, 11], where a much simpler algorithm was used. For the sake of brevity, in this paper we have just included the new and most complex case, the star. This image consists of six orthogonal sine half-waves, each of them with an arbitrary radius. Under this scenario the diffusion field experiments variations with the three coordinate axes and there exists a crossing region. Three different tracking results are shown in Fig. 4 (b), right, each of them for a different seed V_0

It can be seen how the algorithm can be designed in order to pass through isotropic zones where different fiber

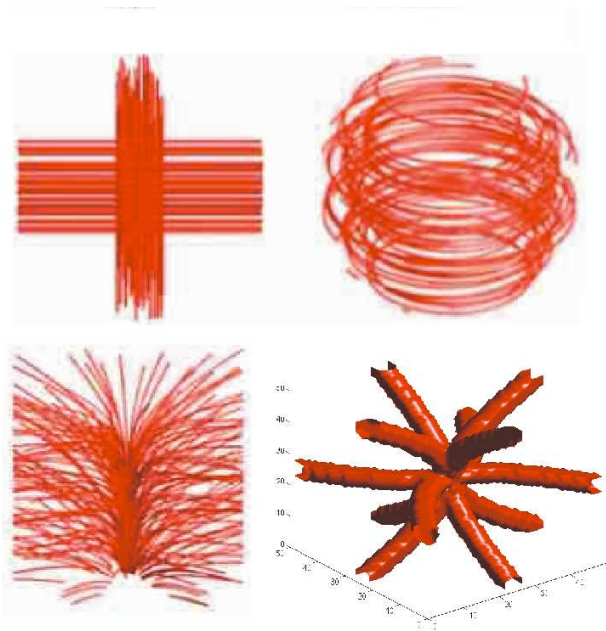


Figure 3: Synthetic DT-MR images used for testing the proposed algorithm: “cross” (left), “earth”, “log” and “star” (right).

bundles cross. It is also appreciated how the algorithm differentiates between the totally isotropic zones extrinsic to the tracts and the fiber bundles.

The differentiation between voxels belonging to a fiber or to a very isotropic area, respectively, is attained by mapping the path probabilities given by Eq. (4) into a color scale and classifying them according to some fixed thresholds. Three different seeds (S_1 , S_2 and S_3) are shown. S_1 and S_2 belong to the intrinsic volume (voxels with a very high anisotropy) and the algorithm moves through the most probable direction following the main direction of the cross in each situation. On the other hand, when an extrinsic point such as S_3 is selected as seed, the algorithm explores in the neighboring voxels until it finds a voxel with a high anisotropy value (point P_1). Once P_1 is found, the tracking algorithm proceeds as in the case of S_1 and S_2 . Fig. 4 shows how the algorithm finds the proper fiber path whatever (extrinsic or intrinsic) seed voxel is chosen.

Notice that, the extrinsic seeds S_3 are located far away from the fiber bundles region, thus making the algorithm explore a wider range of points before reaching the points P_1 that belong to an existing fiber path.

Next, the robustness of the tracking algorithm is now studied for: (i) parameter s is fixed during the whole estimation of the path, and (ii) parameter s is dynamically changed depending on the anisotropy.

- Parameter s fixed. The convergence performance

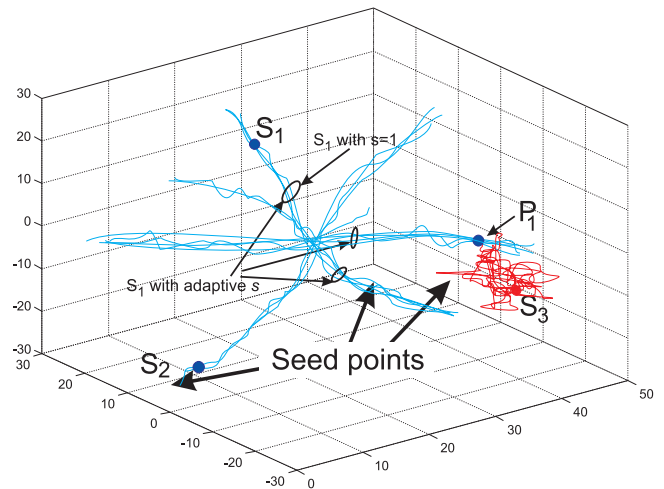


Figure 4: Tracking results for the “star” synthetic DT-MR image. Green: seed points. Blue: fiber path voxels. Red: extrinsic voxels. Initial seeds $V_0 = \{S_1, S_2, S_3\}$.

for different SNRs is shown in Table 1. It can be seen how the algorithm converges properly within a wide range of SNRs. The percentages obtained for the “cross” and the “earth” test images are very close, while for the “log” case the algorithm exhibits a slightly lower convergence. Notice that this table also shows the results for a third method used for comparison¹ [5]. Comparing both methods, we see that the proposed algorithm performs slightly better when the SNR is low, while both methods tend to similar results with high SNRs.

- Parameter s depends on the anisotropy. Fig. 4 (b) also shows the results for the “star” image when: (i) $s = 1$ and (ii) $s = f(\text{anisotropy})$, as explained in section 2.5.

Analyzing the simulations of the four synthetic images considered, it is seen that convergence results improve whenever the MR image contains branching or crossing areas –as it is the case in real DT-MR images. This is the case of our “cross” image. For this image, the convergence results are improved $\sim 5\%$ when parameter s is modified according to the anisotropy. Besides, for these studied cases, we see that the influence of the procedure that adapts s is higher for low SNRs. In case the SNR of the image is large, this procedure scarcely affects the results.

Consequently, the algorithm converges properly within a very wide range of SNRs. The percentages obtained for the “cross” and the “earth” test images are very close, while for the “log” case the algorithm exhibits a slightly

¹The Bayesian algorithm implemented for comparison is a slightly modified version of the method proposed in [5]. This stands for the results given in Tables 1 and 2.

		SNR (dB)					
		5	10	15	20	25	30
Image	Cross	78.3/ 82.8	89.7/ 93.6	92.1/ 94.3	98.3/ 98.7	99.0/ 99.0	100/ 100
		76.8	89.0	90.7	97.0	100	100
	Earth	77.7/ 76.2	88.6/ 87.5	89.9/ 89.0	98.2/ 98.2	99.0/ 99.0	100/ 100
		74.4	83.2	85.0	97.3	99.2	100
	Log	71.0/ 69.7	82.1/ 81.0	86.1/ 85.5	96.0/ 95.8	98.0/ 97.8	100/ 100
		68.8	78.3	85.2	96.0	98.0	100

Table 1: Convergence performance for different SNRs values. Cell values represent percentage of right convergence for two configurations of the algorithm: $s = 1/s = 4$, as well as the results obtained with [5].

lower convergence. Besides, when parameter s is on-line tuned-up the robustness of the algorithm in branching and crossing situations becomes more flexibly controlled and the computational load can be maintained to its lowest value for the kind of desired estimation.

Next, Table 2 shows a computational load comparison with respect to [5]. Values are normalized to the time required by our method with $s = 1$ considering the “cross” image.

	Proposed algorithm				Method [5]
	$s = 1$	$s = 6$	$s = 9$	Adaptive s $1 \leq s \leq 12$	
Cross	1	2.1	3.2	4.9	18.9
Earth	1	2.1	3.2	4.9	20.1
Log	1.1	2.1	3.3	5.0	19.9
Star	1.1	2.2	3.3	5.1	20.0

Table 2: Comparison of computational load. Execution times required to estimate 20 fibers of 200 points. Values normalized to the first case shown (the proposed method with $s = 1$ and “cross” image).

The Bayesian approach of [5] requires much more computational time and resources, while it does not get better convergence results (see Table 1) than the proposed algorithm with fixed or adaptive s . Furthermore, it can be seen that the computational load of the proposed procedure does not increase linearly with the size of the surviving seeds’ pool, s .

3.2 Real images

To conclude this paper, we have applied the proposed tracking algorithm to real DT-MR images. Specifically, we have selected the *corpus callosum* of the brain (Fig. 5) and the fiber pathways in the optic radiations (Fig. 6).

Simulation results are shown on the right. It can be appreciated how the algorithm is able to follow the main fiber bundle direction without getting out of the area of interest. These figures show some bundles of properly es-

timated tracts. Red/green color indicates high/low certainty.

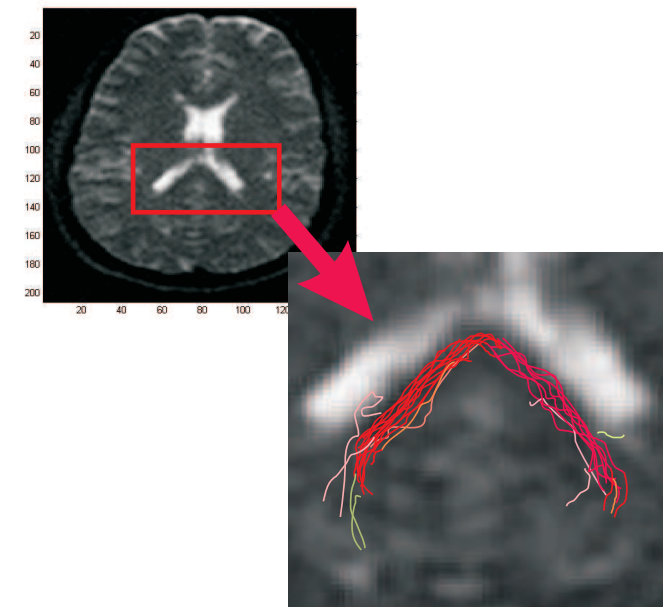


Figure 5: Tracking results for the *corpus callosum* area of the human brain.

The NN-based procedure was useful when changing the volume being analyzed. For instance, with just 8-12 training steps, in synthetic images, or 18-20, in real images, the parameters of the algorithm are fine-tuned so as to get satisfactory results. It is interesting to note that, the choice of the Mahalanobis distance in the RBF basis function allows some advantages over the Euclidean one due to the non-spherical shape of the multidimensional clusters (highly non-linear problem).

Future work will focus on: semiautomatic selection of seeds, improvement of visualization characteristics, development of a user-friendly interface, and study of different techniques and criteria to create and maintain the pool of “future seeds” (directly related to the behavior in crossing and branching regions).

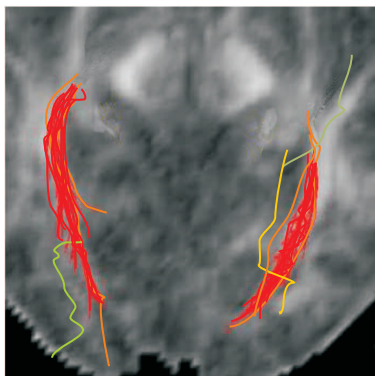


Figure 6: Tracking results for the optic radiation. Seeds are selected lateral to each of the lateral geniculate nuclei.

4 Conclusions and Future Work

A fiber tracking algorithm has been improved and tested with several synthetic and real DT-MRI data. This algorithm combines both the probability of advancing in a specific direction based on the projection of all the eigenvectors components into the corresponding directions (making use of more information than merely the principal eigenvector) and four smoothness criteria based on the relation between the voxels and eigenvectors' orientations. The number of possible paths emerging from the actual point is on-line adjusted based on the local anisotropy. Numerical simulations show that the two main consequences of this are: (i) a better use of computational resources, and (ii) a better performance in regions with crossing or branching fibers. The method was tested with synthetic and real DT-MR images with notably satisfactory results, showing better computational and convergence properties than already existing Bayesian methods. Finally, a brand new NN-based scheme has been proposed for the estimation of the parameters of the algorithm, a task that has been heuristically approached in our previous and other authors' works.

5 Acknowledgements

The authors acknowledge the Spanish CICYT for research grant TEC2004-06647-C03-01, as well as the European Commission for the funding associated to the Network of Excellence SIMILAR (FP6-507609).

References

[1] Bjornemo, M., Brun, A., "White Matter Fiber Tracking Diffusion Tensor MRI," *Master's Thesis*, Linköping University, 2002.

[2] Conturo, T.E., Lori, N.F., Cull, S.T. *et al.*, "Tracking Neuronal Fiber Pathways in the Living Human Brain," *Proc. of the National Academy of Sciences*

of the United States of America, pp. 10422-10427, 1999.

[3] Coulon, O., Alexander, D.C., Arridge, S.R., "Diffusion Tensor Magnetic Resonance Image Regularization," *Medical Image Analysis*, pp. 47-67, 8/04.

[4] Ehrlicke, H.H., Klose, U., Grodd, U., "Visualizing MR Diffusion Tensor Fields by Dynamic Fiber Tracking and Uncertainty Mapping," *Computers & Graphics*, pp. 255-264, 30/06.

[5] Friman, O., Westin, C.-F., "Uncertainty in White Matter Fiber Tractography," *Proceedings of the MICCAI 2005, LNCS 3749*, pp. 107-114, 2005.

[6] Gudbjartsson, H., Patz, S., "The Rician Distribution of Noisy MRI Data," *Magnetic Resonance in Medicine*, pp. 910-914, 34/95.

[7] Kang, N., Zhang, J., Carlson, E.S., Gembris, D., "White Matter Fiber Tractography Via Anisotropic Diffusion Simulation in the Human Brain," *IEEE Transactions on Medical Imaging*, pp. 1127-1137, 24/05.

[8] Kindlmann, G., Weinstein, D., Hart, D., "Strategies for Direct Volume Rendering of Diffusion Tensor Fields," *IEEE Transactions on Visualization and Computer Graphics*, pp. 124-138, 6/00.

[9] Mori, S., van Zijl, P.C.M., "Fiber Tracking: Principles and Strategies - A Technical Review," *Nuclear Magnetic Resonance in Biomedicine*, pp. 468-480, 15/02.

[10] San-José-Revuelta, L.M., Martín-Fernández, M., Alberola-López, C., "A New Method for Fiber Tractography in Diffusion Tensor Magnetic Resonance Images," *Proc. of the IEEE Int'l Conf. on Signal and Image Processing, ICSIP'06*, Karnataka, India, pp. 380-385, I/06.

[11] San-José-Revuelta, L.M., Martín-Fernández, M., Alberola-López, C., "A New Proposal for 3D Fiber Tracking in Synthetic Diffusion Tensor Magnetic Resonance Images," *Proceedings of the IEEE Int'l Symp. on Signal Processing and its Applications, ISSPA '07*, Sharjah, United Arab Emirates, 2007.

[12] Westin, C.-F., Mainer, S.E., Mamata, H., Nabavi, A., Jolesz, F.A., Kikinis, R., "Processing and Visualization for Diffusion Tensor MRI," *Medical Image Analysis*, pp. 93-108, 6/02.